Relating STM, ARPES, and Transport in the Cuprate Superconducting State

D.J. Scalapino,[1,*] T.S. Nunner,[2,†] and P.J. Hirschfeld[2,‡]

[1] *Department of Physics, University of California Santa Barbara, CA 93106-9530 USA*

[2] *Department of Physics, University of Florida Gainesville, FL 32611 USA*

(Dated: February 2, 2008)

We discuss a wealth of data from various types of experiments which together suggest that the superconducting state of optimally to overdoped BSCCO-2212 can be well-described by the BCS theory with a d-wave gap together with small-angle scattering from out-of-plane defects. These include scanning tunnelling Fourier transform spectroscopy observation of nanoscale inhomogeneity in the local gap edge position, the narrowing of the antinodal ARPES spectrum when BSCCO becomes superconducting, as well as the behavior of the microwave and thermal conductivities. We suggest that the large amount of small-angle scattering in BSCCO can account for the differences between the superconducting properties of BSCCO and YBCO.

PACS numbers: 74.72.-h,74.25.Jb, 74.20.Fg

I. INTRODUCTION

Much of our understanding about the one-electron properties of the cuprate superconducting state derives from experiments on one material, BSCCO-2212, which cleaves between two BiO layers to reveal atomically flat surfaces suitable for scanning tunnelling microscopy (STM) and angle-resolved photoemission spectroscopy (ARPES). Many properties of this system differ quite substantially from the other most-studied cuprate, YBCO-123, and it is important to understand the differences which can be attributed to details of electronic structure and disorder in order to extract universal aspects of cuprate superconductivity. In recent years, high-resolution STM experiments have opened up new windows on local aspects of electronic structure, and raised questions about the role of disorder [1, 2, 5]. In particular, they have revealed inhomogeneities in electronic structure at biases around the gap scale on length scales of 25-30Å. Whether these patchy structures, whose distribution changes with doping, are a result of phase separation in a correlated electronic system [6], or merely a reflection of local doping disorder, is still an open question.

Measurements of the ARPES spectrum of $Bi_2Sr_2CaCu_2O_8$ also raised important questions regarding the role of disorder. Experiments showed the clear emergence of a $d_{x^2-y^2}$-like gap in the superconducting state of BSCCO. In the region of the antinodeal fermi surface these studies revealed a broadened normal state spectrum which was found to sharpen dramatically in the superconducting state [7, 8, 9, 10]. Abrahams and Varma [11] suggested that a major component of the normal state broadening arose from small-angle elastic scattering due to out-of-plane disorder, while a smaller contribution arose from dynamic inelastic scattering. While the inelastic scattering rate was expected to decrease below Tc as the superconducting gap opened, the origin of the apparent collapse of the *elastic* scattering rate was unclear.

There has been also a longstanding puzzle regarding the very different microwave conductivity temperature dependence observed in the YBCO-123 [12] and BSCCO-2212 [13] systems. The much smaller size of the maximum conductivity and the insensitivity to changes in GHz microwave frequency in BSCCO suggest that it is a much dirtier system than YBCO; on the other hand, the data exhibits a large residual $T \to 0$ component and a peak at very low temperatures, in contradiction to the usual picture of the conductivity of a dirty d-wave system. The thermal conductivity [14], on the other hand, appears more standard, with a peak in $\kappa(T)$ near T_c; the relative contribution of phonons and electrons to the thermal current is not directly known, however, so one can make no empirically based statements about κ_{el} directly without a theory of the material.

In this paper, we present a short review of work on the aforementioned spectroscopies of BSCCO-2212 which, when taken together, suggest to us that accounting for the way BSCCO is doped can allow one to construct a unified picture of this fascinating material and resolve many of the remaining puzzles. The presence of interstitial O dopants in the BiO layer, together with many other types of defects away from the CuO_2 plane, make this indeed a dirty material, we believe. On the other hand, the distance of the defects from the CuO_2 plane allows for some screening, resulting in a rather smooth and weak random potential landscape experienced by quasiparticles moving in the plane and lead to small-angle scattering. In addition, in-plane disorder can lead to strong (near-unitary) elastic scattering and dynamic spin-fluctuations lead to inelastic scattering which is sup-

*Electronic address: djs@vulcan2.physics.ucsb.edu
†Electronic address: nunner@phys.ufl.edu
‡Electronic address: pjh@phys.ufl.edu

pressed below T_c. We now explore the consequences of this picture.

II. STM DATA

A. FT-STS Patterns

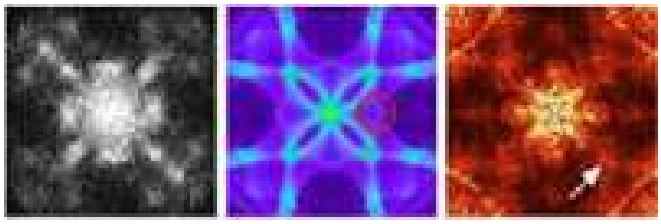

FIG. 1: a) Fourier transform STM image from [2] on a 640Å square of BSCCO-2212 surface at a voltage bias of −14meV;. b) Theoretical $\rho(\mathbf{q},\omega)$ at −14 meV with a single point-like impurity. Red circle denotes position of expected $\mathbf{q}_1$ peak from octet model. c) Many impurity simulation from [16] at −14meV with 0.2% strong impurities ($V = 30t$, with t the near-neighbor hopping) and 8% weak extended impurities ($V = 2t$, range $\sim a$). Arrow indicates position of background feature.

Among the many fascinating aspects of recent Fourier transform - scanning tunnelling spectroscopy (FT-STS) experiments [2, 5] on BSCCO, we focus here on the apparently mundane question of the size of the spots observed in the Fourier pattern, generally taken to represent the local density of states $\rho(\mathbf{q},\omega)$ in the CuO_2 plane, seen e.g. in the first panel of Fig. 1. The various spots in the picture have been claimed to correspond to the so-called "octet vectors", the set of $\mathbf{q}$ connecting points of high density of states at the tips of the curved elliptical contours of constant quasiparticle energy [2]. The single-impurity calculation of $\rho(\mathbf{q},\omega)$[3, 4], although it reproduces correctly the positions of many of the octet vectors and their dispersions, fails to correctly reproduce the weights of these features, and misses some entirely, such as the $\mathbf{q}_1$ peak which should fall inside the red circle in Fig. 1b. In addition, the peaks are extremely sharp relative to experiment. One might anticipate that adding more impurities would broaden the peaks into the observed broad spots in Fig. 1a, but the simplest calculation of many weak impurities gives [15]

$$\delta\rho(\mathbf{q},\omega) \simeq -V(\mathbf{q})\mathrm{Im}\ \Lambda_3(\mathbf{q},\omega)/\pi, \qquad (1)$$

where $V(\mathbf{q})$ is the spatial Fourier transform of the many-impurity potential, and Λ_3 is a response function of the clean system with poles at the positions $\mathbf{q}$ of the octet vectors similar to Fig. 1b. Since $V(\mathbf{q})$ is a random function of $\mathbf{q}$ for a large number of impurities, we see that as disorder increases there is no broadening of the $\rho(\mathbf{q},\omega)$ peaks, but rather an increasing level of the noise floor until the peaks are swamped. A similar result can be obtained for strong point-like impurities[16]. Thus the only possibility to explain the widths of the peaks in these experiments is to assume that the relevant impurities are quite extended. This is not a new concept: for some time studies of T_c supression in the cuprates have suggested that most of the impurities away from the CuO_2 planes must act as small-angle scatterers with little effect on T_c. We believe that STM is now seeing the local consequences of the presence of these scatterers.

B. Nanoscale Inhomogeneity

The nanoscale inhomgogeneity at biases close to the bulk gap edge observed in BSCCO STM experiments have been widely interpreted as strong local fluctuations of the superconducting order parameter with length scale of order 25-30 Å, leading to many scenarios of competing order in the cuprates. While this may indeed be true, and recent observations of charge ordering in "patches" characteristic of underdoped samples have lent support to this point of view [17, 18], it is worthwhile remembering that the STM measures quasiparticle excitations rather than superconducting order, and that quasiparticle interference effects arising from the background disorder potential can also lead to similar signatures. One of the most remarkable aspects of the STM measurements is that they are completely *homogeneous* at biases up to about 20 meV, suggesting that nodal quasiparticles propagate freely without regard for the fluctuations which are causing the nanoscale inhomogeneity at higher energies. It is the antinodal quasiparticles which appear disordered. To illustrate this point, in Fig. 2 we show a "gap map" depicting the position of the 'coherence peak" in a simulation (numerical solution of the Bogoliubov-de Gennes equations [16]) of many impurities in a 2D d-wave superconductor. In this particular simulation, only weak extended impurities were used. As is well known, such defects do not cause resonant behavior at subgap energies; hence the low-energy STM spectrum (also shown) is completely homogeneous. On the other hand, the coherence peak is seen to be quite distorted, with regions of both high and low gap. In this particular case, the range of coherence peak position oscillations is comparable to but smaller than observed in experiment. However, it is noteworthy that this simulation was performed assuming a *constant* order parameter; fluctuations in the coherence peak position in the presence of disorder may therefore involve interference effects which are not necessarily directly related to the order parameter itself. We expect this may be particularly true in the optimally to overdoped materials, where the concentration of the charge-ordered patches is negligible.

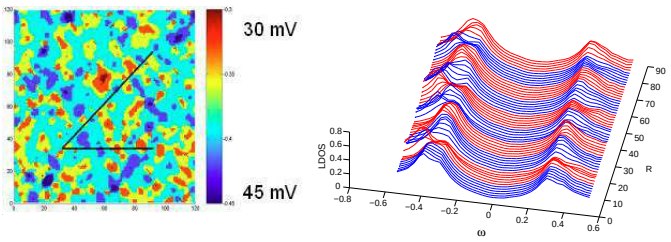

FIG. 2: Left: "gap map" indicating position of negative bias coherence peak from numerical solution of the Bogoliubov-de Gennes equations in the presence of 3% impurities with strength $V = .22t$. Right: local density of states (LDOS) along a horizontal cut through part of the map.

III. ARPES

The ARPES spectrum for the basic model described in the introduction has been discussed in detail in [19]. Here we review this, focusing on the behavior of the small-angle elastic scattering contribution. In the normal state just above T_c, both the small-angle scattering and the spin-fluctuation inelastic scattering lead to a broadening of the single particle spectral weight. Now we know that the inelastic spin- fluctuation scattering is suppressed as the temperature drops below T_c and the gap opens [12, 20]. The question is therefore, what happens to the small-angle elastic scattering? In this case, the momentum averaging over the Fermi surface, which leads to pairbreaking for isotropic impurity scattering, is reduced. In particular, for states near the Fermi surface, which are away from the nodes, one approximately recovers Anderson's theorem [21] and the broadening due to the forward elastic scattering is suppressed in the superconducting state.

In [19], this physics was illustrated with a model where impurity potentials decayed exponentially, $V(r) \propto \exp(-\kappa r)$. The limit $\kappa \to 0$ corresponds to pure forward scatterering, but realistic values are closer to 1 in units of a^{-1}. Scattering was treated in the self-consistent Born approximation. In the case where the elastic scattering is predominantly forward and $\mathbf{k}$ is on the Fermi surface, the Green's function may be written as [20,17]

$$G(\mathbf{k}_F,\omega) = \frac{\omega}{\omega^2 - \Delta(\mathbf{k}_F)^2 + i\Gamma_0(\mathbf{k}_F)\sqrt{\omega^2 - \Delta(\mathbf{k}_F)^2}} \tag{2}$$

Here $\Gamma_0(\mathbf{k}_F)$ is the normal state elastic scattering rate for $\mathbf{k} = \mathbf{k}_F$. Then for $\mathbf{k}_F$ at the antinodal point $\mathbf{k}_A$, shown in the inset of Fig. 3, the spectral weight varies as

$$A(\mathbf{k}_A,\omega) = \frac{\Delta(\mathbf{k}_A)}{\pi\Gamma_0(\mathbf{k}_A)\sqrt{\omega^2 - \Delta(\mathbf{k}_A)^2}} \tag{3}$$

while in the normal state

$$A(\mathbf{k}_A,\omega) = \frac{\Gamma_0(\mathbf{k}_A)}{\omega^2 + \Gamma_0(\mathbf{k}_A)^2} \tag{4}$$

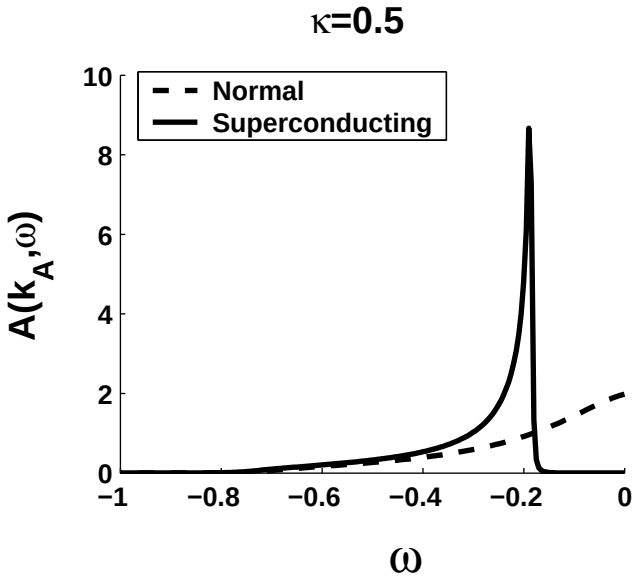

FIG. 3: Spectral function $A(\mathbf{k},\omega)$ for forward elastic scattering in the normal state (dashed) and superconducting state (solid). Here, $\Gamma_0(k_A) = \Delta(k_A) = 0.2t$ and the scattering range parameter $\kappa = 0.5$. The frequency ω is measured in units of the near-neighbor hopping t. The inset shows the upper quadrant of the Brillouin zone and the antinodal point $\mathbf{k}_A$.

Figure 3 shows the normal state spectral weight (dashed) and the superconducting spectral weight (solid) for $\omega < 0$ with $\Gamma_0(\mathbf{k}_A) = \Delta_0$. The ARPES intensity would have a fermi factor multiplying $A(k,\omega)$ which would round off the dashed curve leaving a broad response in the normal state. One clearly sees the suppression of the broadening in the superconducting state. Thus, a sharp spectral gap feature in the ARPES spectrum for $\mathbf{k}_A$ at temperatures below T_c need not be in conflict with having a broad spectrum in the normal state.

IV. MICROWAVE CONDUCTIVITY

Treating extended impurities in the calculation of transport is complicated by the necessity of including vertex corrections to the current-current correlation functions. These are known to vanish at $q = 0$ for point-like scatterers in the d-wave state, but are nonzero if the scattering is anisotropic. This technical difficulty was circumvented by Durst and Lee [23], who linearized the quasiparticle dispersion at the node, and parametrized the anisotropic elastic scattering potential $V_{\mathbf{k}\mathbf{k}'}$ by three independent amplitudes V_α, $\alpha = 1, 2, 3$ for a quasiparticle near one node of the d-wave order parameter to scatter to all four nodes. This treatment renders the problem finite-dimensional, and predicts the breakdown of the universal microwave conductivity at $T \to 0$, $\omega \to 0$. In this case, the $T \to 0, \omega \to 0$ limit of the conductivity is

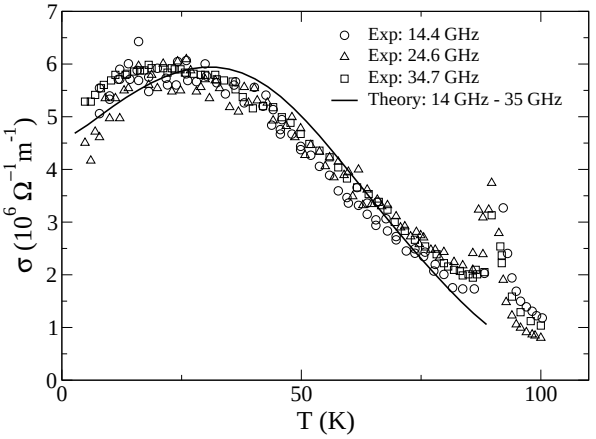

FIG. 4: Microwave conductivity of BSCCO-2212. Data at 3 frequencies from [13], theoretical curve from [24]. Inelastic scattering rate calculated within spin-fluctuation framework adopted from [25], elastic rate calculated using 11% weak impurities with scattering parameters $V_1 = 3t$, $V_2 = 0.4t$, $V_3 = 0.2t$ and 0.05% unitarity limit scatterers.

given by

$$\sigma_0 = \frac{e^2}{\pi^2}\frac{v_F}{v_g}\left(\frac{V_1^2 + 2V_2^2 + V_3^2}{2V_2^2 + 2V_3^2}\right), \qquad (5)$$

where v_F and v_g are the Fermi and gap velocities, respectively. In the isotropic limit, the universal value $\frac{e^2}{\pi^2}\frac{v_F}{v_g}$ (which turns out to be small in the cuprates, of order $0.1 - 0.3\ \sigma(T_c)$) is recovered. Anisotropic scattering (unequal V_α's) implies a value of σ_0 larger than the universal value, and the conductivity diverges in the forward scattering limit $V_2 = V_3 = 0$, $V_1 \neq 0$. In BSCCO, the most striking aspect of the measured microwave conductivity, as shown in Fig. 4, is in fact the apparent large finite value of σ_0.

Nunner and Hirschfeld [24] recently extended this technique to finite frequencies and temperatures, treating strong pointlike impurities within the t-matrix approximation, weak extended ones within the Born approximation, and evaluating the total vertex function. Although this technique is most suited for low T, and expected to yield only semiquantitative results near T_c, good agreement is obtained (Figure 4) with a model consisting of inelastic scattering from spin fluctuations identical to that used to explain data on YBCO, plus roughly the same percentage of strong and weak extended scatterers that was used to fit the STM data. Calculations for YBCO show that good fits can be obtained over the entire range of frequencies and temperatures if the scatterers are assumed to be strong, but have a small scattering range. Thus the microwave data confirms the general picture that the defect type and spatial distribution are quite different in YBCO and BSCCO crystals.

V. THERMAL CONDUCTIVITY

Finally we turn our attention to the thermal conductivity, where the vertex corrections play a less important role, and small-angle scattering processes contribute significantly to the transport lifetime. While these corrections actually vanish at zero temperature, they contribute at nonzero T, although they remain small. To demonstrate consistency with the discussion of the previous experiments, we compare in Fig. 5 calculated results with the data of Ando *et. al* [14]. The peak heights and normal state values of both the nominally pure and Zn-doped sample are comparable to those seen in experiment, although the theoretical calculation is for only the electronic part of the conductivity [24]. From these fits it appears that, in contrast to YBCO, the phononic contribution to the thermal conductivity in BSCCO must be quite small relative to the electronic contribution near T_c, whereas it dominates the transport at temperatures around $10K$. The reduced relevance of the vertex corrections for this quantity means that the large concentration of intermediate strength scatterers broadens quasiparticle states and leads to a temperature dependence similar to the standard "dirty d-wave" model.

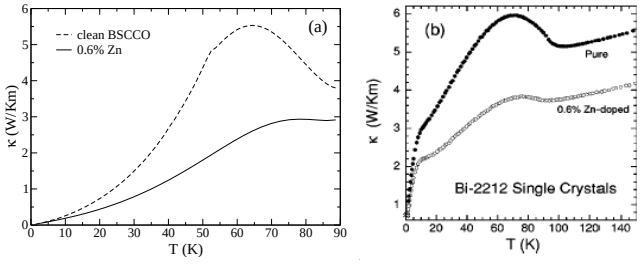

FIG. 5: Thermal conductivity of BSCCO-2212. (a) Theoretical curve from [24] for $\kappa_{el}(T)$. Inelastic scattering rate calculated within spin-fluctuation framework adopted from [25], elastic rate calculated using 11% weak impurities with scattering parameters $V_1 = 3t$, $V_2 = 0.01t$, $V_3 = 0.001t$ and 0.05% unitarity limit scatterers (upper curve). Lower curve has 0.6% additional unitarity scatterers. (b) Data on optimally doped BSCCO-2212 single-crystal [14]. Upper curve: nominally pure sample, lower curve: 0.6% Zn.

VI. CONCLUSIONS

Here we have argued that small-angle elastic scattering from out-of-plane impurities can alter the electronic properties of the cuprate superconductors and that this can account for differences between BSCCO and YBCO. The weak Van der Waals coupling between the BiO layers in BSCCO, which allow it to cleave so nicely for ARPES and STM measurements, also provides a region in which disorder can occur leading to small-angle elastic scattering of the carriers in the CuO_2 layers. Here we have argued that when this small-angle scattering is taken into

account, along with the usual in-plane impurity and inelastic spin-fluctuation scattering, one can understand the differences between the superconducting properties of BSCCO and YBCO.

Acknowledgments

The authors thank W.A. Atkinson, L.-Y. Zhu and T. Dahm for numerical calculations and enlightening discussions. Partial support was provided by ONR N00014-04-0060 (PJH), NSF-DMR02-11166 (DJS), and the A. von Humboldt Foundation (TSN).

[1] A. Yagdani, *et. al*, *Phys. Rev. Lett.* **83**, 176 (1999).
[2] J.E. Hoffman *et. al*, *Science* **295**, 466 (2002); K. McElroy *et. al*, *Nature* **422**, 592 (2003).
[3] Degang Zhang and C. S. Ting, Phys. Rev. B 67, 100506 (2003).
[4] Qiang-Hua Wang and Dung-Hai Lee, Phys. Rev. B **67**, 020511 (2003).
[5] C. Howard, *et. al*, *Phys. Rev. B* **64**, 100504 (2001).
[6] V.J. Emery and S.A. Kivelson, *Phys. Rev. Lett.* **72**, 1918 (1994).
[7] Z.-X. Shen, *et. al*, *Phys. Rev. Lett.* **70**, 1553 (1993).
[8] J.M. Harris, *et. al*, *Phys. Rev. Lett.* **79**, 143 (1997).
[9] J.C. Campuzano, *et. al*, *Phys. Rev. Lett.* **83**, 3709 (1999).
[10] A. Damascelli, Z. Hussain, and Z.-X. Shen, *Rev. Mod. Phys.* **75**, 473 (2003).
[11] E. Abrahams and C.M. Varma, *Proc. Nat'l Acad. Sci.* **97**, 5714 (2000).
[12] A. Hosseini, R. Harris, S. Kamal, P. Dosanjh, J. Preston, R. Liang, W.N. Hardy, and D.A. Bonn, *Phys. Rev. B* **60**, 1349 (1999).
[13] Shih-Fu Lee, D.C. Morgan, R.J. Ormeno, D.M. Broun, R.A. Doyle, J.R. Waldram, and K. Kadowaki, *Phys. Rev. Lett.* **77**, 735 (1996).
[14] Y. Ando, J. Takeya, Y. Abe, K. Nakamura, and A. Kapitulnik, *Phys. Rev. B* **62**, 626-630 (2000).
[15] L. Capriotti, D.J. Scalapino, and R.D. Sedgewick, *Phys. Rev. B* **68**, 45120 (2003).
[16] L. Zhu, W.A. Atkinson, P.J. Hirschfeld, *Phys. Rev. B* **69**, 060503 (2004).
[17] J.E. Hoffman, *et. al*, *Science* **295**, 466 (2002).
[18] M. Vershinin, *et. al*, *Science*
[19] L.-Y. Zhu, P.J. Hirschfeld, and D.J. Scalapino; cond-mat/0406304.
[20] D. Duffy, D.J. Scalapino, and P.J. Hirschfeld, *Phys. Rev. B* **64**, 224522 (2001).
[21] P.W. Anderson, *Phys. Rev. Lett.* **3**, 328 (1959).
[22] R.S. Markiewicz; cond-mat/0309254.
[23] A.C. Durst and P.A. Lee, *Phys. Rev. B* **62**, 1270 (2000).
[24] T.S. Nunner and P.J. Hirschfeld, unpublished.
[25] S. M. Quinlan, D. J. Scalapino, and N. Bulut, *Phys. Rev. B*, **49**, 1470 (1994).